9-14-2012

Serpentine Low Loss Trapezoidal Silica Waveguides on Silicon

Xiaomin Zhang

Mark Harrison

Audrey Harker

Andrea M. Armani

Serpentine Low Loss Trapezoidal Silica Waveguides on Silicon

Serpentine low loss trapezoidal silica waveguides on silicon

Xiaomin Zhang,[1,3] Mark Harrison,[2,3] Audrey Harker[1] and Andrea M. Armani[1,2,*]

[1]*Mork Family Department of Chemical Engineering and Materials Science, University of Southern California, Los Angeles, California 90089, USA*

[2]*Ming Hsieh Department of Electrical Engineering-Electrophysics, University of Southern California, Los Angeles, California 90089, USA*

[3]*These authors contributed equally to this work.*

[*]*armani@usc.edu*

Abstract: We report the fabrication and characterization of straight and serpentine low loss trapezoidal silica waveguides integrated on a silicon substrate. The waveguide channel was defined using a dual photo-lithography and buffered HF etching and isolated from the silicon substrate using an isotropic silicon etchant. The waveguide is air-clad and thus has a core-cladding effective index contrast of approximately 25%. Measured at 658, 980 and 1550nm, the propagation loss was found to be 0.69, 0.59, and 0.41dB/cm respectively, with a critical bending radius less than 375μm. The waveguide's polarization behavior was investigated both theoretically and experimentally. Additionally, the output power shows a linear response with input power up to 200mW.

OCIS Codes: (130.3120) Integrated optics devices; (130.2790) Guided waves.

References and links

1. C. Kopp, S. Bernabe, B. B. Bakir, J. Fedeli, R. Orobtchouk, F. Schrank, H. Porte, L. Zimmermann, and T. Tekin, "Silicon photonic circuits: On-CMOS integration, fiber optical coupling, and packaging," IEEE J. Sel. Top. Quantum Electron. **17**, 498–509 (2011).
2. A. Himeno, K. Kato, and T. Miya, "Silica-based planar lightwave circuits," IEEE J. Sel. Top. Quantum Electron. **4**, 913–924 (1998).
3. Y. Vlasov and S. McNab, "Losses in single-mode silicon-on-insulator strip waveguides and bends," Opt. Express **12**, 1622–1631 (2004).
4. J. F. Bauters, M. J. R. Heck, D. John, D. Dai, M.-C. Tien, J. S. Barton, A. Leinse, R. G. Heideman, D. J. Blumenthal, and J. E. Bowers, "Ultra-low-loss high-aspect-ratio Si3N4 waveguides," Opt. Express **19**, 3163–3174 (2011).
5. T. C. Sum, A. A. Bettiol, J. A. van Kan, F. Watt, E. Y. B. Pun, and K. K. Tung, "Proton beam writing of low-loss polymer optical waveguides," Appl. Phys. Lett. **83**, 1707–1709 (2003).
6. T. Miya, "Silica-based planar lightwave circuits: passive and thermally active devices," IEEE J. Sel. Top. Quantum Electron. **6**, 38–45 (2000).
7. G. L. Bona, R. Germann, and B. J. Offrein, "SiON high-refractive-index waveguide and planar lightwave circuits," IBM J. Res. Develop. **47**, 239–249 (2003).
8. X. Zhang and A. M. Armani, "Suspended bridge-like silica 2x2 beam splitter on silicon," Opt. Lett. **36**, 3012–3014 (2011).
9. A. J. Maker and A. M. Armani, "Low loss silica on silicon waveguides," Opt. Lett. **36**, 3729–3731 (2011).
10. J. F. Bauters, M. J. R. Heck, D. D. John, J. S. Barton, C. M. Bruinink, A. Leinse, R. G. Heideman, D. J. Blumenthal, and J. E. Bowers, "Planar waveguides with less than 0.1 dB/m propagation loss fabricated with wafer bonding," Opt. Express **19**, 24090–24101 (2011).
11. T. C. Hansuek Lee, J. Li, O. Painter, and K. J. Vahala, "Ultra-low-loss optical delay line on a silicon chip," Nat. Commun. **3**, 1 (2012).
12. F. Ladouceur and E. Labeye, "A new general approach to optical waveguide path design," J. Lightwave Technol. **13**, 481–492 (1995).
13. E. A. J. Marcatili, "Bends in optical dielectric guides," Bell Syst. Tech. J. **48**, 2103–2132 (1969).
14. I. H. Malitson, "Interspecimen comparison of the refractive index of fused silica," J. Opt. Soc. Am. **55**, 1205–1208 (1965).
15. D. Derickson, *Fiber Optic Test and Measurement* (Prentice Hall, 1997).
16. P. K. Tien, "Light waves in thin films and integrated optics," Appl. Opt. **10**, 2395–2413 (1971).

#173345 - $15.00 USD Received 26 Jul 2012; revised 21 Aug 2012; accepted 12 Sep 2012; published 14 Sep 2012

17. A. Boskovic, S. V. Chernikov, J. R. Taylor, L. Gruner-Nielsen, and O. A. Levring, "Direct continuous-wave measurement of n_2 in various types of telecommunication fiber at 1.55 mm," Opt. Lett. **21**, 1966–1968 (1996).
18. K. Schmitt, B. Schirmer, C. Hoffmann, A. Brandenburg, and P. Meyrueis, "Interferometric biosensor based on planar optical waveguide sensor chips for label-free detection of surface bound bioreactions," Biosens. Bioelectron. **22**, 2591–2597 (2007).
19. H. K. Hunt and A. M. Armani, "Label-free biological and chemical sensors," Nanoscale **2**, 1544–1559 (2010).
20. A. L. Washburn and R. C. Bailey, "Photonics-on-a-chip: integrated waveguides as enabling detection elements for lab-on-a-chip biosensing applications," Analyst (Lond.) **136**, 227–236 (2011).

1. Introduction

Integrated waveguides are one of the fundamental elements of photonic circuits [1, 2]. The two key factors of a high performance waveguide are low propagation loss and small bending radius. Previous research has demonstrated waveguides integrated on silicon substrates based on various materials such as silicon, silicon nitride, polymers and silica [3–10]. Of these, silica is an ideal material for most photonic applications, as it inherently has ultralow loss from the visible through the near-IR. In comparison with semiconductor materials, it has extremely low nonlinear behavior, such as the Kerr Effect, and thus enables high power transfer. Typically, the refractive index contrast between the core and the cladding in silica waveguides is small (less than 1.5 percent). This restricts the bending radius to several mm, and thus limits achieving smaller footprints. By increasing the refractive index contrast, more compact devices are possible, enabling denser photonic circuit using silica devices [6]. However, the current methods of increasing the index contrast involve complex and expensive fabrication processes, such as depositing additional and often dissimilar materials [4–6]. Therefore, achieving large index contrast silica waveguides with simple fabrication methods is a laudable goal. However, despite recent advances in the field of integrated silica photonics which leverage ultra-low loss oxides, the majority of work to date is unable to direct and confine light in arbitrary directions [11].

In this work, a suspended trapezoidal silica waveguide is directly fabricated on a silicon substrate with a simple two step photo-lithography and buffered HF etching. Both straight waveguides and serpentine waveguides were characterized at 658, 980 and 1550nm, and the structure was modeled using both finite difference time domain (FDTD) and finite element method simulations. As a result of the trapezoidal shape, the device is able to effectively confine light in both straight and serpentine shaped bends. Additionally, the waveguide's polarization behavior was investigated both theoretically and experimentally. At 1550nm, the power-dependent performance was measured up to 200mW. Because the suspended silica waveguide is air-clad, the effective refractive index difference is approximately 25%.

2. Experimental methods and modeling

2.1 Device fabrication

To thoroughly characterize the behavior of the trapezoidal waveguide, both straight and serpentine devices were fabricated. The fabrication and characterization of the serpentine devices which contain both inside and outside bends is critical in thoroughly understanding the behavior of this new waveguide geometry. Previous research with integrated silica waveguides has focused on spiral devices which only have outside bends, mimicking resonant cavities [11]. However, optical circuit design cannot be limited to structures which only curve in one direction. Therefore, to fully explore the potential of silica waveguides for these applications, it is necessary to understand and be able to predict its behavior.

The trapezoidal silica waveguides are fabricated from 2μm thick thermal oxide (wet) on a 300μm silicon wafer (Montco Silicon). The fabrication process for the trapezoidal silica waveguide is shown in Figs. 1(a)-1(c). First, 80μm wide silica rectangles are defined using a combination of photolithography and buffered oxide etching using buffered hydrofluoric (HF) acid (Fig. 1(a)). It is important to note that the trapezoidal shape (in the z-axis direction) arises as a result of the inherent isotropic nature of the buffered HF etching process. It is

#173345 - $15.00 USD Received 26 Jul 2012; revised 21 Aug 2012; accepted 12 Sep 2012; published 14 Sep 2012

possible to control the various angles in the trapezoid by balancing the exposure time to hexamethyldisilazane (HMDS), which occurs before the deposition of the photoresist, and the concentration of the buffer used to create the buffered HF.

Next, a second photolithography and buffered HF etching step are used to carve out two 8-µm wide trapezoids at each side of the 80µm trapezoids (Fig. 1(b)). The photolithography and buffered HF etching process are optimized to create trapezoids with 45 degree sidewall. The trapezoidal waveguides are then diced using a diamond scribe to create the input and output ends. In order to isolate the lower refractive index silica waveguide from the higher refractive index silicon substrate, XeF_2 etching was used to undercut the silica until the silicon pillar is approximately 10µm away from the waveguides (Fig. 1(c)). A schematic of the cross section is shown in Fig. 1 (d). While w, W and h were held constant at 64 µm, 80 µm and 2 µm respectively, the membrane thickness varied between 900 nm and 1 µm.

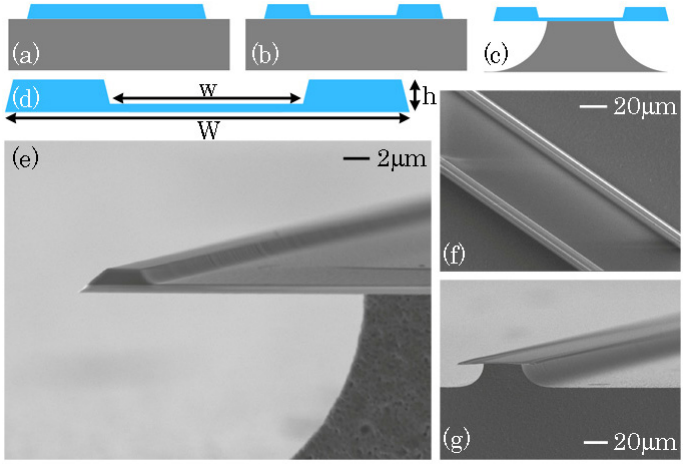

Fig. 1. Fabrication process and scanning electron micrograph (SEM) images of the trapezoidal waveguide. (a) 80µm wide silica trapezoids are defined using photolithography and buffered HF etching.(b) A second photolithography and buffered HF etching are used to create two 8µm trapezoids at each side of the 80-µm trapezoids, and (c) XeF_2 etching is used to isotropically undercut the silica.(d) Cross section schematic of the waveguide indicating the critical dimensions. In the present experiments, W = 80µm, w = 64µm and h = 2µm. (e) SEM side view image of a single waveguide, (f) top view image of a pair of waveguides, (g) SEM side view image of a pair of waveguides.

Figures 1(e)-1(g) are SEM images of the trapezoidal waveguide. Figure 1(e) is the zoomed in image of one trapezoidal waveguide. It is important to note that the ends are quite smooth, which is verified by measuring the coupling loss. Figure 1(f) is the top view of the complete trapezoidal structure. Figure 1(g) is the sideview/ends of the trapezoidal waveguide which shows a pair of trapezoidal waveguides supported by the silicon pillar. Given the dimensions defined in Fig. 1(d), this device supports higher-order modes and operates in a multi-modal fashion. However, by changing the initial masks, it should be possible to optimize this performance, potentially achieving single mode devices. Additionally, although the present work is focusing on fabricating pairs of waveguides separated by the pillar, by changing the initial photomask, it will be possible to fabricate multiple adjacent waveguides or single waveguides.

Serpentine waveguides are also fabricated using this process. An S-curve geometry (Fig. 2) is chosen in order to study the effect of both outside and inside bending on the optical field. The inside bending radius (R) is varied from 125 to 400µm at 25µm increments, yielding twelve different curved devices. The length of the waveguide arms is held constant to allow straightforward calculation of the bending loss.

#173345 - $15.00 USD Received 26 Jul 2012; revised 21 Aug 2012; accepted 12 Sep 2012; published 14 Sep 2012

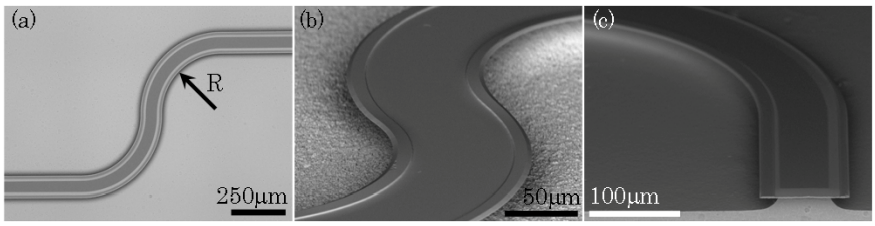

Fig. 2. Scanning electron micrograph (SEM) images of the curved trapezoidal waveguide. (a) The S-curve waveguide geometry depicting the bending radius (R), which was varied between 125 and 400μm. (b) SEM of the bending section and (c) cleaved end of a curved waveguide device.

2.2. Finite element method modeling and finite differential time domain simulations

As shown in Fig. 1 and Fig. 2, the trapezoidal waveguide is suspended off of the silicon substrate by a silica membrane. One concern is that the optical field might leak into the membrane, thereby increasing the overall loss of the device or distorting the mode profile. Therefore, the optical field profile of the fundamental mode of the device was modeled at 658, 980 and 1550nm, using COMSOL Multiphysics finite element method analysis. For comparison, we also modeled silica rectangular and circular waveguides with the same width at the same wavelength. The results at 1550nm for the TE mode are plotted in Figs. 3 (a)-3(c) and used to form Fig. 3(d). The electric field distribution in all three devices is symmetric, indicating that there is minimal leakage into the membrane. However, the effective mode area of the trapezoidal waveguide is significantly smaller than the other geometries.

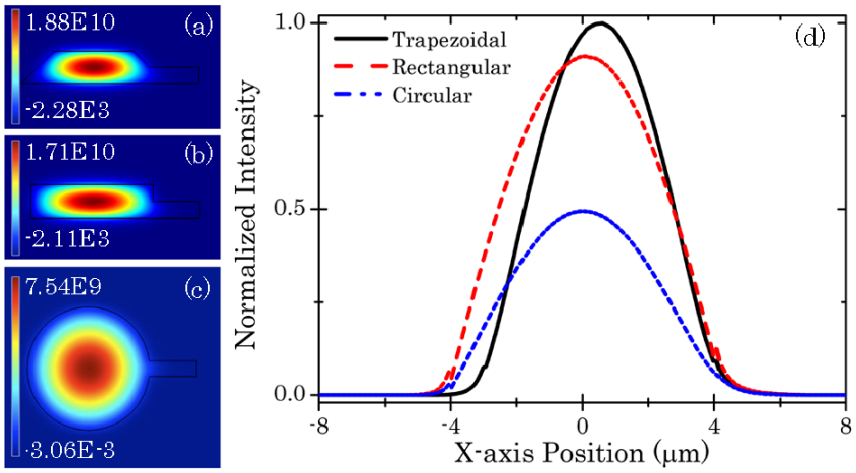

Fig. 3. Finite element method simulation of the electric field distribution (TE mode) of (a) trapezoidal, (b) rectangular waveguide and (c) circular waveguide at 1550nm. (d) Comparison of the intensity of the mode profile along the x (horizontal) direction, normalized to highest intensity in trapezoidal device.

Using these FEM results, the effective refractive indices for the TE and TM polarization states were calculated and they are slightly different for the wavelengths studied, indicating that the device should have polarization dependent operation observable over long propagation distances. Additionally, based on these results, the effective refractive index contrast $((n^2_{core}-n^2_{clad})/(2n^2_{core}))$ of the device is 25.6%, 25.3% and 24.5% at 658, 980, and 1550nm, for the TE modes [12]. The behavior for the TM mode is similar.

#173345 - $15.00 USD Received 26 Jul 2012; revised 21 Aug 2012; accepted 12 Sep 2012; published 14 Sep 2012

Table 1. Comparison of the Effective Refractive Indices of TE and TM Modes

Wavelength (nm)	TE	TM
658	1.4313	1.4305
980	1.4222	1.4199
1550	1.4011	1.3933

One of the present hurdles in developing compact integrated circuits is bending or radiation loss, which results from mode radiation, reflection resulting from phase mismatch, and increased interaction with sidewall roughness. In the present devices, optical field leakage into the supporting membrane also increases radiation loss, as the effective refractive index contrast is slightly asymmetric. One approximation for the bending or radiation loss (α_b) is [13]:

$$\alpha_B \propto \left(\frac{\pi}{\gamma^3 R}\right)^{1/2} \left(\frac{\kappa}{V}\right)^2 \exp\left(-\frac{2}{3}\left(\gamma^3/\beta_g^2\right)R\right) \quad (1)$$

where R is the bend radius, β_g is the propagation constant of the waveguide, V is proportional to the effective refractive index contrast between the core and the cladding. Lastly,κ is proportional to the refractive index of the waveguide, the free space propagation constant and β_g, and γ is proportional to the refractive index of the cladding layer, the free space propagation constant and β_g. One approach for solving this equation is simulating the optical field profile throughout the bend. However, because of the complex three-dimensional profile of the device, it is necessary to use finite difference time domain (FDTD) simulations.

Using Lumerical FDTD, curved devices having similar geometrical values to those fabricated were simulated. Specifically, inner bend radii of 50μm to 175μm, at 25μm increments, as well as one device with an inner bend radius of 250μm operating at 1550nm were modeled. The light travelled first through a 90-degree inside bend followed by a 90-degree outside bend. In order to accurately capture behavior of the waveguides with a 1550nm light signal, we did not use the built in SiO_2 material to draw the structure, but instead used the user-defined dielectric material with a refractive index set to 1.444, which is the refractive index of fused silica at 1550nm [14]. Using a mode source object, we injected the fundamental mode of the straight waveguide into the waveguide arm that goes through an inner bend first. We used the mode of the straight waveguide in order to capture the mode-mismatch loss that will be present in the experimental results, as we coupled light into a straight portion of the waveguide first during experiments.

In order to determine the loss in the simulations, we used two 2D Y-normal frequency-domain power monitors, one close to the source and one at the very end of the waveguide. Additionally, we used one 2D Z-normal monitor to capture the field profile in the overview of the entire structure. The monitor at the output was used to measure the power going out of the far waveguide arm, P_{out} which was used to easily calculate the loss in dB. Finally, the loss was divided by the arc-length of the waveguide arms through which the light travelled in order to normalize the loss at each bending radius to dB/cm. Because of the way the loss was measured and calculated, the simulation loss results are directly comparable to the experimental results.

Unfortunately, we were unable to include the silicon pillar in our simulations. From the simulations, as light travels through an inside bend of a curved waveguide, a significant amount of the optical field leaks into the membrane (Fig. 4.). When this occurs, a portion of this field may be lost into the silicon pillar, which has a higher refractive index than the silica membrane and waveguides.

#173345 - $15.00 USD Received 26 Jul 2012; revised 21 Aug 2012; accepted 12 Sep 2012; published 14 Sep 2012

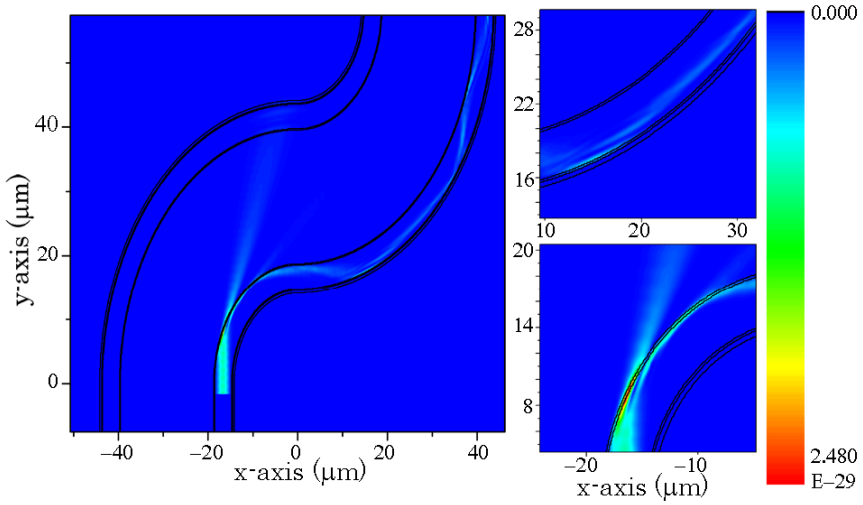

Fig. 4. Finite-difference time-domain simulation of the electric field intensity bent trapezoidal waveguide with an inner radius of 75μmat 1550nm. The optical field clearly leaks into the silica membrane in-between the two waveguide arms. This leakage is a significant source of loss in the serpentine devices.

2.3 Experimental setup

To characterize the waveguide, a single mode lensed fiber (Oz Optics) with a spot size of around 2μm is used to couple light into the waveguide. A series of fixed wavelength diode lasers at 658, 980, and 1550nm were used for the initial optical loss measurements performed at moderate input powers. The alignment process is monitored using both a top and side view vision systems. For precise alignment with the waveguide, the lensed fiber is mounted on a nanometer resolution XYZ motorized stage (Newport). The output light from the waveguide is directly focused into a power meter (InGaAs) or an optical beam profiler which is part of an M^2 Beam Quality Analysis system (InGasAs detector, Thor Labs) by an aspheric lens, instead of using an additional lensed fiber. Eliminating the output lensed fiber results in lower coupling loss and fewer alignment errors, and thus enables a more accurate measurement of the device performance. To accurately determine the loss, the cut-back method was used [15]. Both straight and serpentine waveguides were tested using this setup.

A complementary high input power measurement was also performed on straight waveguides. For this experiment, a 1550nm laser is connected to an erbium doped fiber amplifier (EDFA). The output of the EDFAis connected to a 99:1 optical coupler. The 1% output is monitored by a power meter and the 99% output is connected to the lensed fiber and coupled into the waveguide. The power coming out from the waveguide is focused into the beam profiler. A free space attenuator is inserted between the focal lens and beam profiler to avoid saturating the beam profiler.

Finally, at 1550nm, the polarization dependent loss is determined by varying the polarization of input light by placing an inline polarization controller between the laser and the lensed fiber. Specifically, the output power from the waveguides and the input power from the lensed fiber at several polarization states are recorded.

3. Experimental results and discussion

3.1 Propagation loss measurement

The propagation loss is measured using the cut-back method which assumes constant coupling loss and uniform surface roughness. The transmission loss (dB) from the

#173345 - $15.00 USD Received 26 Jul 2012; revised 21 Aug 2012; accepted 12 Sep 2012; published 14 Sep 2012

waveguides over a series of different lengths is plotted and then fitted to line to get the propagation loss (dB/cm). The loss at a given device length is defined as [15]:

$$Loss\,(dB) = -10\log\left(\frac{P_{out}}{P_{in}}\right) \tag{2}$$

where P_{in} is the input power and P_{out} is the output power from the waveguide. Figure 5 is the loss measurement results. The propagation loss is 0.69, 0.59 and 0.41dB/cm at 658, 980 and 1550nm respectively as determined from the slope of the linear fit. The coupling loss is also determined by the intercept which is [2.3, 1.6, 1.3]dB at [658, 980, 1550]nm. As mentioned earlier, this waveguide supports higher order modes, so the loss measurement is not for fundamental mode only. It is important to note that these are straight waveguides which were several mm long, not devices in ring geometries. Therefore, it is anticipated that the bandwidth would be similar to that of optical fiber. Additionally, the results from multiple devices are shown, verifying the reproducibility of the measurements.

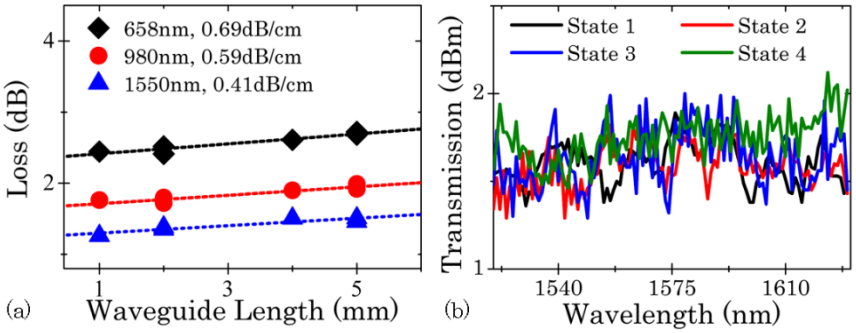

Fig. 5. (a) Measured propagation loss of the trapezoidal silica waveguide at three wavelengths: 658, 980 and 1550nm.(b) Transmission at four different polarization states.

As proposed by Tien [16], the propagation loss α is defined as:

$$\alpha = \frac{\sigma^2 k_0{}^2 h}{\beta}\frac{E_s{}^2}{\int E^2 dx}\Delta n^2 \tag{3}$$

where σ is the core/cladding interface roughness, k_0 is the free space wavenumber, β is the modal propagation constant, Δn is the refractive index difference between the core and the cladding, h is the transverse propagation constant in the core, and E_s is the scattered electric field amplitude due to surface roughness. As shown in Eq. (3), the propagation loss is proportional to the scattered electric field amplitude E_s. There are two dominant loss regimes: 1) reduction in optical mode confinement, and 2) surface scattering due to roughness. At long wavelengths, when the optical mode approaches the size of the device, the first regime is the dominant loss mechanism of the device. At shorter wavelengths, interface roughness is the primary loss mechanism. As can be clearly observed from the simulation results, the optical mode is completely confined within the device. Additionally, the loss increases as the wavelength decreases. Therefore, the increase in propagation loss is the result of an increase in the scattered electric field amplitude due to interface roughness (σ) [3].

Figure 5(b) shows the results from the polarization measurements. The transmission at different polarization states varied slightly, which indicates that the waveguide has a small polarization dependence over long propagation lengths. However, it is important to note that the multi-modal behavior of the waveguide also means that these devices are not polarization-maintaining. Due to this behavior, the polarization dependence of the devices is not useful, as small changes in things like input coupling conditions can have an effect on the polarization

#173345 - $15.00 USD Received 26 Jul 2012; revised 21 Aug 2012; accepted 12 Sep 2012; published 14 Sep 2012

state of the light within the waveguide. Although the simulation results for the effective refractive indices for the TE and TM polarizations indicate polarization-dependent behavior(Table 1), experimentally we see that due to the multimodal behavior of the waveguides, the polarization dependence is somewhat unpredictable. In Fig. 5(b), the transmission for various polarization states fluctuates somewhat randomly, often overlapping, indicating that this unpredictable behavior does not have a large effect for standard operation of these waveguides. By modifying the device dimensions but keeping the overall geometry similar, it might be possible to achieve single mode operation and make the polarization dependence more useful.

3.2. Bending loss

The bending loss of the curved waveguide was calculated using the following relationship:

$$\alpha_{total} = \alpha_{length} + \alpha_{system} + \alpha_{bend} \tag{4}$$

where α_{total} is the total measured loss of the devices, α_{length} is the loss due to waveguide length, α_{system} is a constant that consists primarily of coupling loss, and α_{bend} is the bending loss. The total loss is found by measuring the difference between the input and output powers, as detailed previously. Losses due to length (α_{length})are found by measuring the length of the curved device (R) and measuring the length of the arms using an optical microscope. This total length is multiplied by the propagation losses of 0.69, 0.59 and 0.41dB/cm at 658, 980 and 1550nm, which are found above. To account for length differences, the loss was normalized by dividing the measured loss in dB by the arc-length of the waveguide bends. The length loss and the system loss are then subtracted from the total loss to calculate the bending loss.

Figure 6 shows the bending loss as a function of bending radius. Each point represents a unique device (N>3 for each R). For all three wavelengths, the loss is fit to an exponential curve. From Fig. 6, one can see that the exponential fits for all three wavelengths are very similar, with the shorter wavelengths exhibiting more loss. This occurs because at shorter wavelengths, the light more easily leaks into the silica membrane and is therefore more easily lost into the silicon pillar. If the light signal were to only travel through outside bends, we expect that this trend might be reversed. The critical bending radius has a slight wavelength dependence, and is below 375μm for all wavelengths.

For direct comparison, the simulation results are also plotted in Fig. 6. While the general shape of the results is in excellent agreement with the experimental values, the precise bending loss values are systematically lower. As mentioned previously, the simulations did not include the silicon pillar. This difference provides further support for the hypothesis that the leakage into the membrane and the subsequent loss into the silicon pillar accounts for a significant portion of our bending losses. Therefore, if the light signal only travelled through outside bends, the bending loss would be much lower and the critical radii would be significantly reduced, due to the high index contrast of the devices, and our simulations support this theory.

#173345 - $15.00 USD Received 26 Jul 2012; revised 21 Aug 2012; accepted 12 Sep 2012; published 14 Sep 2012

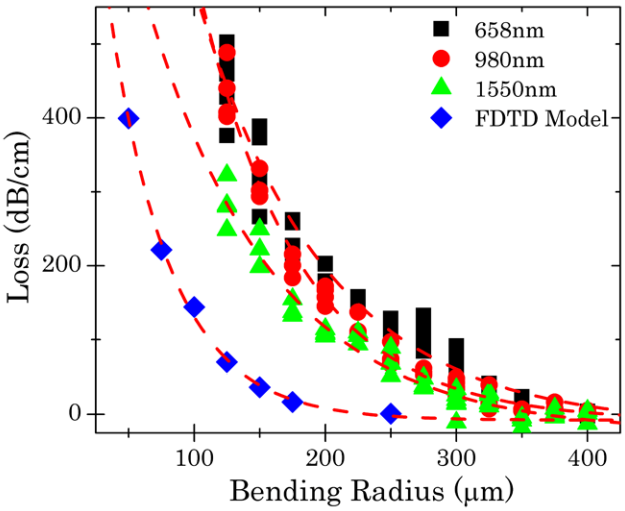

Fig. 6. Measured bending loss of the trapezoidal silica waveguide at 658, 980 and 1550nm and the FDTD results.

3.3 Power dependence

Silica is known to have very low power-dependent, non-linear coefficients [17] from the visible through the near-IR and thus the trapezoidal waveguide should have a linear power response at very high input powers. As shown in Fig. 7, the output power of the trapezoidal waveguide changes linearly with the input power up to 200mW, which was the maximum power achievable by the laser input system. This linear behavior is quite an advantage compared with silicon or polymer waveguides which have large power-dependent, non-linear coefficients. The fabricated silica waveguide thus shows great potential for high power applications.

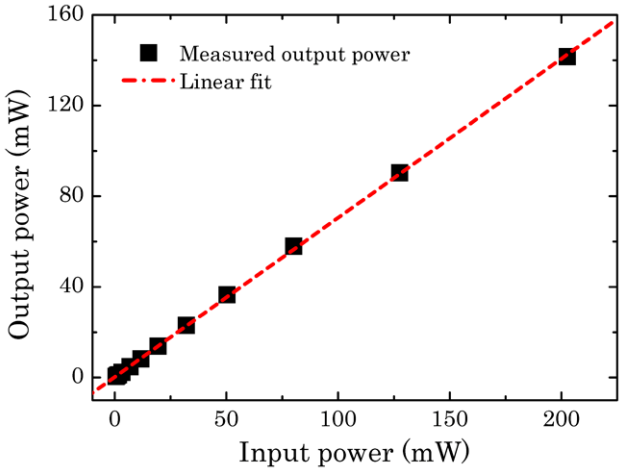

Fig. 7. The output power of the trapezoidal waveguide shows a linear dependence on the input power up to 200mW.

5. Conclusion

In conclusion, straight and serpentine trapezoidal silica waveguides on a silicon substrate are fabricated, modeled and characterized. Finite element method and finite difference time domain simulations accurately model the device behavior from the visible through the near-

#173345 - $15.00 USD Received 26 Jul 2012; revised 21 Aug 2012; accepted 12 Sep 2012; published 14 Sep 2012

IR and predict the observed slight polarization-dependent behavior, as well as excellent optical field confinement. The trapezoidal shape pinches the optical mode, resulting in a reduction in the effective mode area. As a result of the high effective refractive index contrast and the low optical loss of silica, the loss measured using the cut-back method is 0.69, 0.59 and 0.41 dB/cm at 658, 980 and 1550nm, respectively, and the critical bending radius was below 375μm for all wavelengths. Additionally, the waveguide has a linear power response up to 200mW. This structure is very simple and inexpensive to fabricate with the advantage of an extremely high core-clad effective refractive index contrast (25%). As such, this type of suspended trapezoidal waveguide geometry will find applications in integrated photonics [1, 2], and bio/chemical sensing [18–20].

Acknowledgments

The authors thank Yang Yue and Prof. Alan Willner for the EDFA measurements. M. Harrison is supported by a NDSEG fellowship. This work was supported by ONR (N00014-11-1-0910). Additional information is available at http://armani.usc.edu.

#173345 - $15.00 USD Received 26 Jul 2012; revised 21 Aug 2012; accepted 12 Sep 2012; published 14 Sep 2012